An Effective Control Technique to Implement an IUPQC Design for Sensitive Loads in a Hybrid Solar PV-Grid Connection

OLUWAFUNSO OLUWOLE OSALONI[1], AYODEJI STEPHEN AKINYEMI[2], ABAYOMI ADURAGBA ADEBIYI[2], AYODEJI OLALEKAN SALAU[1,3]

[1]Department Electrical Electronic and Computer Engineering, Afe Babalola University Ado Ekiti, Ekiti-State, NIGERIA
[2]Department Electrical Power Engineering, Durban University of Technology, Durban, SOUTH AFRICA
[3]Saveetha School of Engineering, Saveetha Institute of Medical and Technical Sciences, INDIA

Abstract: - The recent innovation in power electronic application in the electrical power system (EPS) has given birth to an Improved Unified Power Quality Conditioner (IUPQC) that positively impacts the electrical power system (EPS). The previously available mitigation approaches with the application IUPQC are monotonous and are major designs for a particular power quality (PQ) issue which does not take care of the degree of impart. This paper presents an effective control architecture of an IUPQC design for sensitive loads in hybrid Photovoltaic Solar (PV) connected grid, concentrating on the voltage demand of loads that respond to slight changes. The objective of this work is to design a flexible controller that can respond to the different degrees of PQ challenges concerning voltage, variable load, and solar irradiation. It has combined the merits of an IUPQC and grid-integrated PV source. Effective controllers for Voltage Source Inverter (VSI) connected in series and Current Source Inverter (CSI) connected in shunt compensators of the UPQC are implemented to increase device strength for different voltage and current distortions. The series compensator was controlled using an enhanced Synchronous Reference Frame (SRF) technique based on adaptive notch filters. An Adaptive Logarithmic Absolute Algorithm (ALAL) was deployed for the parallel section of the proposed approach. The Mean Turning Filter (MTF) was used as a replacement for a low pass filter (LPF) for direct current node voltage management, leaving high and low-frequency ripples unaffected. To maintain a constant current on the grid side during grid disturbances, a feed-forward element has been introduced to the shunt CSI controller. Under various network situations, such as under-voltage, over-voltage, voltage distortion, harmonics, rapid load changes, and fluctuation in solar power, the control system performance is better as confirmed by experimental validation. Finally, it is observed that the voltage profile of 0.984 p.u. due to application control falling within the permissible limits. The proposed controllers are tested in the MATLAB Simulink on a developed distribution system model and validated experimental prototype.

Keywords: - Solar Photovoltaic, Under-voltage, Voltage Sensitive Load (VSL), Over-voltage, Unbalance voltage, improved unified power quality conditioner.

Received: June 28, 2022. Revised: January 9, 2023. Accepted: February 15, 2023. Published: March 17, 2023.

1 Introduction

The advancement in power electronics results in various nonlinear loads at the load center, making the distribution system increasingly prone to many power quality issues, [1], [2]. A lot of power conditioners have been proposed to achieve the electricity value requirements in the distribution network. Traditional UPQCs have proven their ability to tackle a variety of PQ challenges among all types and capacities of power quality conditioners, [3], [4], [5]. Researchers have proposed diverse power conditioners and UPQC in response to various power system concerns. The presence of diverse types of loads and voltage fluctuation at the receiving end resulted in PQ challenges, and there is a need for a mitigation device in the distribution grid. Because current harmonics cannot be reduced, the work, [6] proposed a voltage amelioration approach for critical loads to protect them from voltage fluctuation. A repeatable controller with a recursively least square technique was used in the series compensator. The effective voltage restorer used for loads with voltage sensitivity, [7], and [8] suggested a controller centered on an improved phase-locked loop (PLL).

Quite enough research has been carried out on electric grid disruption prevention strategies to

address (PQ) concerns such as distortion, imaginary power improvement, dynamic routing, grid current mitigation, flicker reduction, under voltage reduction, and over-voltage advancement, [8], [9]. [6] proposed the application of a dynamic voltage restorer (DVR) to safeguard vulnerable loads from power supply variations. Although the loads examined are voltage and current-vulnerable loads that can exist in the grid and were not resolved, [4], [6], [8], [9], [10]. The work done in, [13], [14] suggested a specific UPQC architecture with a series inverter at the receiving end to reduce voltage signal alterations. For nonlinear and VSLs, [11], [12], left shunt UPQC (LS-UPQC) is deployed in a single-phase network for current and voltage distortions. The LS-UPQC was used to eliminate simultaneous voltage and current disturbances from recent work in the literature. Due to numerous groups of customers with different power quality requirements at the point of use, they must choose the level of power quality that best fits their budget. The article, [6] also presented the open UPQC design, in which the shunt and series inverters possessed individual dc-link capacitors. This novel architecture can suit customers' needs by providing quality power at distinct levels and varied prices to manage open UPQC. Also, [16], [17], proposed a controller with little arithmetical calculation centered on an upgraded PLL.

The idea of open UPQC has been used by, [18], and [19], for power control in intelligent low-voltage grids. Open UPQC with multilevel ameliorator architecture (O-UPQC-ML) was presented in [20] to showcase the notion of reducing the switching frequency of devices by multilayer compensator and multiple power quality levels supplied by O-UPQC. In [21], a novel O-UPQC architecture for VSL with DVRs mounted at specified load branches. Since renewable energy is on the verge of grid absorption, power conditioners are being used in distribution networks in a transitional phase. As investigated and implemented in [15], [16], the incorporation of solar photovoltaic (PV) sources into the grid via distributed static ameliorator (DSTATCOM) has gained favour in maintaining current related PQ issues. Photovoltaic solar interconnected with UPQC devices have received a lot of consideration in the past few years. To tackle concurrent grid challenges, the effective use of PV-UPQC in these research investigations results in a favorable level of PQ improvement, [18], [19], [21]. However, the provision of various electricity quality levels to end customers at varied price levels has remained unaffected.

Furthermore, because the conventional device enhances PQ for all end-users in the distribution system, [19], the design fails to allow the customer to select diverse PQ levels. There is a requirement for a multifunctional device that can merge clean power generation with power quality enhancement. This is due to the request for clean energy and sophisticated electronic loads demanding power quality. The publications, [6], [20], offer a 3-phase multipurpose solar energy conversion system that accounts for load-side PQ concerns at a different stage. However, this custom device enhances voltage levels for all connected customers in the electricity grid, these topologies fail to give freedom for the customer to pick alternative power quality levels.

This work offers a potential solution to the end-user for all the PQ difficulties and varying PQ levels, especially in the presence of loads with voltage sensitivity, to create a distributed voltage controller that allows for greater communication among distributed generators and nearby controllers. The connection of light loads, like computers and information technology (IT) electronics end-user consumers load, who are concerned about better voltage quality, necessitates using a unique form of the power conditioner. This work has proposed a PV-fed IUPQC with PV fed parallel inverter of UPQC at the connection point and VSI branch connected with a load having voltage sensitivity following in PCC 2 as shown in Figure 1. The PV-IUPQC demands more effective controllers for its ameliorators to protect the loads with voltage sensitivity in case of any harmful grid condition at the distribution level. As a result, more efficient and effective controllers were developed and implemented in this paper. The suggested system's execution was evaluated in steady-state with MATLAB and has proven possible to protect critical loads from severe grid voltage disruptions.
Furthermore, current quality difficulties for different load unbalancing scenarios in the distribution system are avoided. The reaction of the system to variations in solar irradiation has also been investigated. The following is how the rest of the article is structured: The suggested PV-IUPQC topology's system setup was included in Section II. Section III carried out a thorough expression of the control algorithms. The simulations and results were showcased in Section IV under different load conditions. Finally, Section V brings this article to a conclusion.

The characteristic of Figure 1 includes the IGBT shunt and series inverter, the series and shunt

transformer, the nonlinear load, inductors, and resistors.

2 Network Framework

The approach proposed in [26], combines PV and UPQC functionality to provide a unique solution for VSLs. As illustrated in Figure 1, [26], the current architecture has the DVR linked near the delicate load and the shunt CSI closer to the primary side. The shunt and series ameliorator in this system uses a common DC-link. Furthermore, the series VSI and the parallel CSI are coupled to the dc-link through the PV.

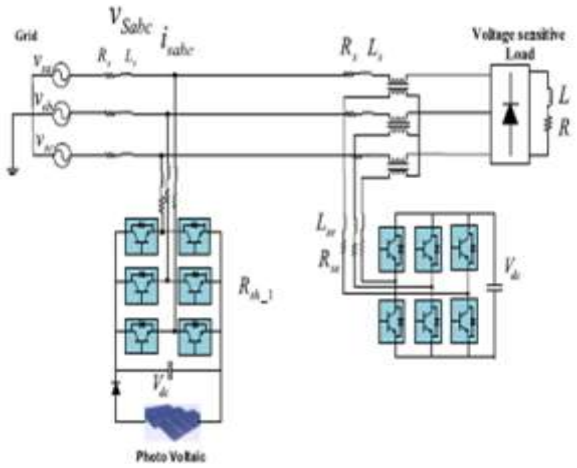

Fig. 1: Topology of PV-IUPQC Architecture, [26]

2.1 Control Design Architecture

The regulated architecture of PV-UPQC's structure for the function of compensators is critical for improving PQ and meeting the demands of end consumers and the distribution network. To sufficiently switch pulses, the control algorithm's overall structure incorporates two primary algorithms: a flexible notch filter centered on synchronous reference frame theory (FNF-SRF) for the VSI and an adjustable logarithmic (AL) for the CSI. The PV source is made linked to the grid via UPQC because the highest power point tracking (HPPT) approach of perturbation and observation (P & O) has been used to harvest full PV power harvested from the PV array.

2.2 VSI Controller

This work has developed a flexible method for the PV-IUPQC controller to increase the execution of the series VSI of the UPQC. Flexible notch filter technology is suggested for the network interconnection of the Synchronous Reference Frame (SRF) controller for series VSI. The flexible notch filter (FNF) was first developed in [22], [23], for accurate grid integration by giving correct core signals even in highly inaccurate grids and removing PLLs from the system's controller. Lately, in [24], FNF was applied to control UPQC because of its flexible disposition to network instabilities. Thus, an FNF-SRF controller has been considered to enhance the controller implementation to produce turning signals for the series VSI of PV-IUPQC. Evaluation of grid voltage in PV interconnection procedures is critical with phase angle; consequently, FNF built synchronization technique is examined in this article as given in Figure 2. The current approach, which runs without a typical PLL, provides an exact and speedy performance in distorted and imbalanced grid circumstances. The flexible notch filter is applied for harmonization, which delivers an appropriate harmonization signal regardless of the disruption in the network. The FNF can be described, [25] with the set of the equation as:

$$\ddot{\eta} + \vartheta^2\eta = 2\gamma\vartheta\varepsilon(t) \quad (1)$$

$$\dot{\vartheta} = -\varphi u\vartheta\varepsilon(t) \quad (2)$$

$$\varepsilon(t) = z(t) - \dot{\eta} \quad (3)$$

where ϑ is the estimated frequency, and γ and φ are adjustable, accurate positive parameters that define the Estimation Accuracy (EA) and the Convergence Speed (CS) of the FNF. The FNF block's input state vector is (η), which comprises the essential and distortion elements. The EA and CS are provided by the FNF differential equations of FNF, which have two variable parameters (γ) and (φ). For a single sinusoid input signal $(n = 1)$, $z(t) = \kappa_1 \mathrm{Sin}(\lambda_1(t) + \varphi_1)$, this ANF has a distinctive periodic and distinctive orbit located at (4):

$$\begin{pmatrix} \eta_1 \\ \dot{\eta}_1 \\ \vartheta \end{pmatrix} = \begin{pmatrix} -\kappa_1 . \frac{1}{\lambda_1} \mathrm{Cos}(\lambda_1(t) + \varphi_1) \\ \kappa_1 \mathrm{Sin}(\lambda_1(t) + \varphi_1) \\ \lambda_1 \end{pmatrix} \quad (4)$$

Figure 2 shows a simple mathematical description of FNF and the controller for a series VSI. The synchronization unit based on FNF can offer details on phase, frequency, phase angle, and harmonic component. The phase angle value in Cos/Sin is extracted using FNF in the current SRF controller. The work in [25], [26] provides a more extensive description of the FNF-based synchronization unit. The advanced adaptive control techniques required in RDS are the central focus of this paper to protect VSLs from voltage variations. The FNF scheme is used in conjunction with the SRF theory to improve

controller efficiency. Even in grid voltage disruptions, the FNF synchronization scheme gives reliable information to the SRF controller. In addition, to increase the elimination of low-frequency ripples, a moving average filter was used in conjunction with a dc-link controller of a series APF.

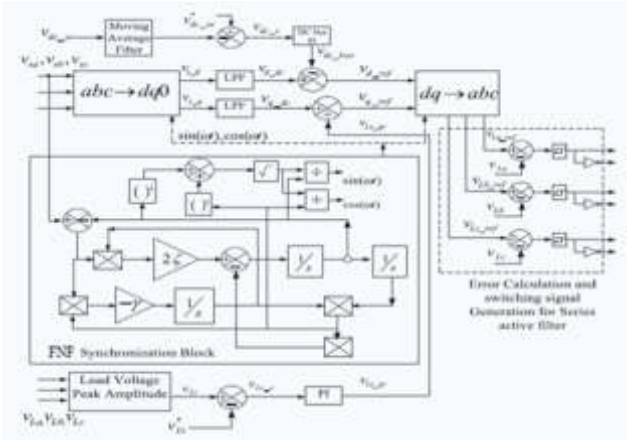

Fig. 2: Series ameliorator for FNF-SRF controller

The PV-IUPQC system has been implemented in this article to suit the voltage quality requirement of a particular end-user. The series ameliorator possesses a self-supporting DC-link and the capacity to inject quadrature voltage. The quadrature voltage compensation is accountable for load imaginary power correction. This function minimizes total reliance on parallel CSI designed for imaginary power compensation. The FNF-based SRF procedure has been used to alleviate voltage disturbances triggered by the series VSI. As illustrated in Figure 3, the standard coupling (PCC) voltage point is identified and then transformed to a d-q-0 frame by applying the park transformation and information from the FNF unit. Low pass filters removed harmonic and oscillating elements from the d-axes and q-axes elements of source voltages. Input voltages' d-axes and q-axes features can be showcased as (5) and (6):

$$v_{1_d} = v_{d\_dc} + v_{d\_ac} \quad (5)$$

$$v_{s\_q} = v_{q\_dc} + v_{q\_ac} \quad (6)$$

where v_{d_dc} and v_{d_ac} are the input voltages for dc and ac components under d-axes, while v_{q_dc} and v_{q_ac} are the input voltages for dc and ac components under q-axes. The self-supported capacitor's dc bus voltage should be adjusted at a constant level to obtain appropriate series compensator performance. The measured DC-Link Voltage (DCLV) is conveyed via a moving average filter (MAF) rather than a fundamental LPF to lower extreme and low-frequency ripples. For the dc voltage control device to extract the dc element, the MAF has been utilized to measure the dc voltage without sacrificing effective implementation. MAF application is deployed for the DCLV management mechanism, [21], [25] for a wind turbine with low power, and, [22] for a power transformation circuit of the fuel cell. On the other hand, this article introduces MAF usage for the PV-IUPQC dc-link mechanism. The MAF transfer function is written as (7):

$$F_{MAF}(s) = \frac{1-e^{-k_w s}}{k_w s} \quad (7)$$

The MAF's window length can be represented as k_w. The filtered output of the MAF device was matched to the reference DCLV, and the inaccuracy found was sent to the dc bus PI regulator. The voltage loss is calculated by employing the output of the PI regulator on the direct current bus. The following formula in (8) and (9) can be utilized to represent the voltage drop acquired for the sample instant point:

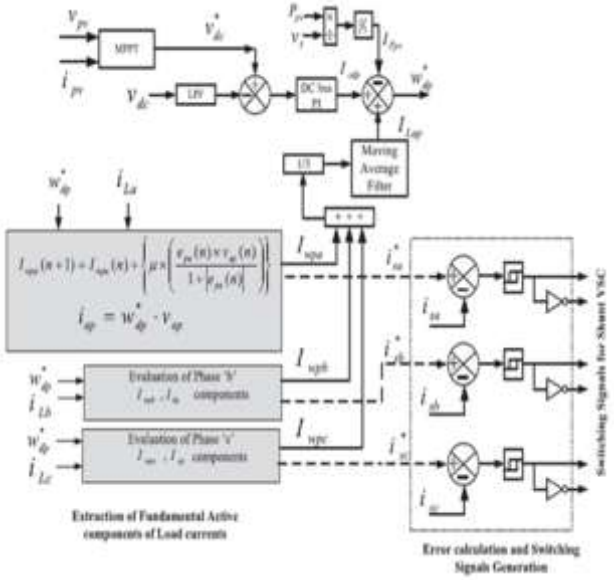

Fig. 3: Flexible for absolute algorithm-based controller for shunt ameliorator

$$v_{dc_e}(n) = v^*_{dc\_se} - v_{dc_{se}}(n) \quad (8)$$

$$v_{dc_{loss}}(n) = v_{dc_{loss}}(n-1) + Y_{p\ \ se1}.(v_{dc_e}(n) - v_{dc_e}(n-1) + Y_{I\_se}.v_{dc_e}(n) \quad (9)$$

where the $v^*_{dc\_se}$ series real filter controller's reference dc voltage, $v_{dc_e}(n)$ is the DCLV inaccuracy, $v_{dc_{loss}}(n)$ is the PI controller's output,

Y_{p_se1} is the relative increase, and Y_{I_se} is the integral increase. As a result, the load voltage (LV) reference d-axis elements can be written as (10):

$$v_{d\_ref} = v_{d\_dc} - v_{dc\_loss} \tag{10}$$

The terminal LV amplitude is calculated using (11):

$$v_{L(t)} = (2/3)^{1/2} \sqrt{v_{La}^2 + v_{Lb}^2 + v_{Lc}^2} \tag{11}$$

where v_{La}, v_{Lb}, v_{Lc} are the voltages per phase at the load terminal, the error produced between the load and reference voltage is sent into the controller after comparison. The imaginary element of the LV $v_{Lt\_qr}(n)$ is quantified at the receiving end of the PI regulation (13). The inaccuracy is regulated by employing the PI voltage controller to offer a reference number to produce the source q-axis element of LV.

$$v_{L(t)_e}(n) = v_{Lt}^{*} - v_{Lt}(n) \tag{12}$$

$$v_{Lt\_qr}(n) = v_{Lt_{qr}}(n-1) + Y_{p\ \ se2}.(v_{Lt_e}(n) - v_{Lt\_e}(n-1)) + Y_{I\_se2}.v_{Lt\_e}(n) \tag{13}$$

The LV, the imaginary element of the voltage at the load terminal combined with the dc filtering element of voltage quadrature in (14):

$$v_{q\_ref} = v_{q\_dc} + v_{Lt\_qr} \tag{14}$$

The source *d*-axis, v_{d_ref} and q-axis element v_{q_ref} of LVs (LVs) are the input to the Inverse Park's transformation (IPT) to evaluate the Reference LVs (RLVs) correspond to as $v_{La_{ref}}$, v_{Lb_ref}, and v_{Lc_ref}. To calculate the reference LVs and the IPT uses the reference and element of LVs. The RLVs contrast to the detected LVs to create inaccuracies sent to the pulse with a modulator (PWM) voltage regulator to produce an electrical signal for the VSI.

2.3 Inverter Active Power Filter Controller

The PV-O-shunt UPQC's compensator controller calculates the source currents for generating a pulse signal for the parallel real power filter. Estimating the Reference Current (RC) gets challenging when there are grid voltage disturbances. As a result, the shunt compensator requires an adaptive controller for typical operations. In [20], multiple adaptive Filtering Algorithms (FAs) are suggested, with the ALAL filtering algorithm demonstrating its permanence in the existence of several network disruptions. Furthermore, due to its compelling character, the fundamental logarithmic purifying technique has previously been employed for a PV-DSTATCOM method in severe weak grid situations, [21]. The ALAL filtering technique can extract fundamental current even during significant grid voltage disruptions. The control algorithm for the Insulated Gate Bipolar Transistor (IGBT) of the parallel real power filter has several subsections, including unit template computation and MAF-based DCLV controller, for appraisal feed-forward term, fundamental real weight element resolution, production of switching signal generation, and the current Reference Signal (RS). Figure 3 depicts the detailed controller, and the phase voltages are in charge of determining the terminal source voltage's amplitude given in (15):

$$v_t = \sqrt{\frac{2}{3}(v_{sa}^2 + v_{sb}^2 + v_{sc}^2} \tag{15}$$

The phase unit models are determined by the ratio of calculated terminal sending end voltage amplitude to per phase voltage in each case

$$v_{ap} = \frac{v_{sa}}{v_t}, \tag{16}$$

$$v_{bp} = \frac{v_{sb}}{v_t}, \tag{17}$$

$$v_{cp} = \frac{v_{sc}}{v_t} \tag{18}$$

Grid disruptions are expected in grid-connected PV systems owing to demand dissimilarity and voltage oscillations at the grid. As a result, even in voltage changes, the feed-forward term must uphold the suitable current at the right level to adjust the power equilibrium. As shown here, the feed-forward pulse of PV, I_{Fpv} is calculated using the amplitude of terminal voltage and the power collected from the PV panel as shown in (19):

$$I_{Fpv} = \frac{2P_{pv}}{3v_t} \tag{19}$$

The feed-forward term ensures that the current at the grid is regulated in the event of voltage variations. Any atmospheric variations reflected in the PV energy source are supplied into the real current element via the feed-forward term. The perceived DCLV is compared to the reference DCLV after passing through an average turning filter to minimize undesired ripples. After passing through a moving average filter, the sensed DCLV is compared to the reference DCLV to minimize undesired ripples. The (P & O) HPPT algorithm

produces the reference DCLV by detecting the PV voltage and PV current. The dc bus PI controller receives the error created by the comparison. The quantified error for the nth sample sudden error produced by the DCLV is expressed in equations (20) and (21):

$$v_{sh_e}(n) = v^*_{dc_{pv}}(n) - v_{dc_{sh}}(n) \quad (20)$$

$$i_{cdp}(n) = i_{cdp}(n) + Y_{psh}v_{sh_e}(n-1) - v_{sh_e}(n) + Y_{ish}(v_{sh_e}(n+1)) \quad (21)$$

where Y_{psh}, and Y_{ish} are the comparative and integral benefits for the PI regulator of the DCLV regulator, with the real loss element of the RC quantified at the PI regulator's production. The output of RC signals is answerable for amelioration in the current system. This necessitates the determination of a helpful reference in altered signal settings that appears to be problematic. Controller adaptation to network voltage perturbations can manage this delicate condition by including an adaptive element in the RC signal assessment process. The outstanding function of the LA filters is assessed, [27], [28]. [29] demonstrated the efficacy of a total logarithmic controller for DSTATCOM. As a result, the writers used this notion in this article for the PV-IUPQC. The proposed logarithmic fundamental algorithm, as described by (22), is used to compute the natural weight element of total Load Current (LC) for phase A:

$$i_{wpa}(n+1) = i_{wpa}(n) + \left\{\epsilon \times \frac{e_{wa}(n)\times v_{ap}(n)}{1+|e_{wa}(n)|}\right\} \quad (22)$$

where the value of ϵ performance error is chosen so that it does not exceed the bound as shown in (27). The appropriate value of ϵ should be considered when extracting the amplitude of the fundamental component of LC. For the supposed system, the current approach performs better at ϵ = 0.018. The error produced by the adaptive integrant of the method under consideration is denoted by e_{wa}. Therefore, each phase can appraise the error as shown in (23) to (27):

$$e_{wa}(n) = i_{La}(n) - v_{ap}.I_{wpa}(n) \quad (23)$$

$$I_{wpb}(n-1) = I_{wpb}(n) + \left\{\mu \times \left(\frac{e_{wb}(n)\times v_{bp}(n)}{1+|e_{wb}(n)|}\right)\right\} \quad (24)$$

$$e_{wb}(n) = i_{Lb}(n) - v_{bp}.I_{wpb}(n) \quad (25)$$

$$I_{wpc}(n-1) = I_{wpc}(n) + \left\{\mu \times \left(\frac{e_{wc}(n)\times v_{cp}(n)}{1+|e_{wc}(n)|}\right)\right\} \quad (26)$$

$$e_{wc}(n) = i_{Lc}(n) - v_{cp}.I_{wpc}(n) \quad (27)$$

The real power element of the dc bus of PV-IUPQC and the average size element of the real power of LC (I_{Lap}), as well as the feed-forward component, can be used to calculate the total weight of the essential fundamental element of the RC as shown in (28):

$$w^*_{dp} = I_{cdp} + I_{Lap} - I_{Fpv} \quad (28)$$

where the following equation has been applied to calculate the average size of the real power element of LC as given by (29):

$$I_{Lap} = \frac{1}{3}\left(I_{wpa} + I_{wpb} - I_{wpc}\right) \quad (29)$$

The RC for each phase is now calculated as follows in (30):

$$i^*_{sa} = w^*_{dp}v_{ap,}\ i^*_{sb} = w^*_{dp}v_{bp,}\ i^*_{sc} = w^*_{dp}v_{cp,} \quad (30)$$

The established RC is equated to the actual detected current. The difference is sent to the hysteresis current controller, which produces switching signals for the PV-IUPQC parallel active filter's insulated gate bipolar transistor.

3 Simulation Results and Discussions

This phase lays the groundwork for intensive simulation experiments to determine the viability of the proposed PV-IUPQC device. The network was created in MATLAB SIMULINK 2021. Its functions were evaluated in various simulation scenarios, including system efficiency under different potential quality problems, dynamic performance under unusual operating voltage, efficient functioning under unbalanced load conditions, and effective performance under solar irradiation variations. Table 1 lists the system parameters that were used in the simulation. The simulation results confirmed the system's efficacy and performance under various dynamic circumstances. The implementation of the developed effective SRF voltage controller is authenticated using a simulation test system and settings from Table 1.

Table 1. Simulation Parameters

Selected Parameters	Values
Voltage @ grid side	220 V
System Standard frequency	50 Hz
Source Inductance	0.5 mH
DC bus capacitor	3.5 mF
Series VSI inductance	0.5 mH
Shunt CSI inductance	3.5 mH
Non-linear load	100 Ω 4mH
Phase load	50 100 85/55mH
Switching frequency	10 kHz
PV power @ MPPT	600 watts
Voltage (Vmp) @ MPPT	220 V
Current (Imp) @ MPPT	2.7 Amp

The opening test shows the planned controller's capacity to track RSs. At t = 0:24s, the d-element of the RS voltage drops to 0:2679 pu, and at t = 0:77 s, the q-element of the RS voltage jumps to 0.217 pu from 0:2524 pu. Figure 4 represents the investigational and simulation results of the standalone microgrid network as a result of these step transitions in load RSs. The effects reveal that the suggested controller has good tracking performance when regulating LVs.

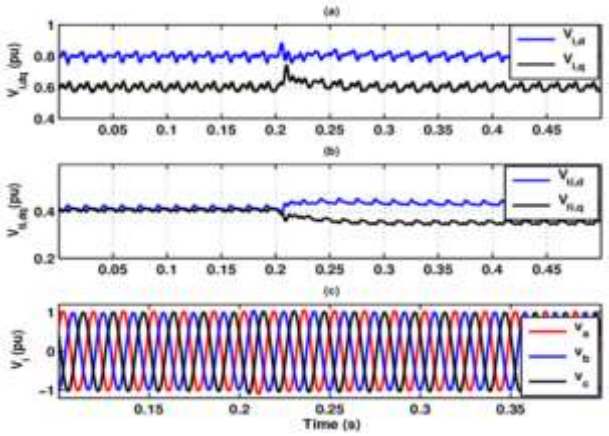

Fig. 4: Effective feedback of test network owing to a purely resistive load change (a) dq-elements of the LV, (b) control inputs, and (c) 3phase LVs

Furthermore, Figure 4 shows that the modelling results match the experimental data. However, owing to the pulse harmonics of the PWM-based Voltage Source Converter (VSC), some ripples in the LVs were noticed in the investigational outcomes. According to IEEE guidelines, [30], [31], the quantity of ripple is acceptable.

The suggested voltage controller manages the d and q elements between 0.79 p.u and 0.59 p.u at LVs, correspondingly, in the second test. As shown in Table 1, the load inductance/capacitance are also set to their nominal standards. At roughly t = 200ms, the LRs in the 3-phases are scaled down similarly from five lamps to zero. The effective reaction of the test network as a result of the resistive load variation is shown in Figure 5. The d and q elements of the LVs were regulated to 0.929 p.u and 0.368 p.u, correspondingly, in the third test. The load inductances in the three phases are suddenly stepped increased from 5mH to 25mH while the Load Resistance (LRs) and Load Capacitance (LCs) are secured at their nominal values.

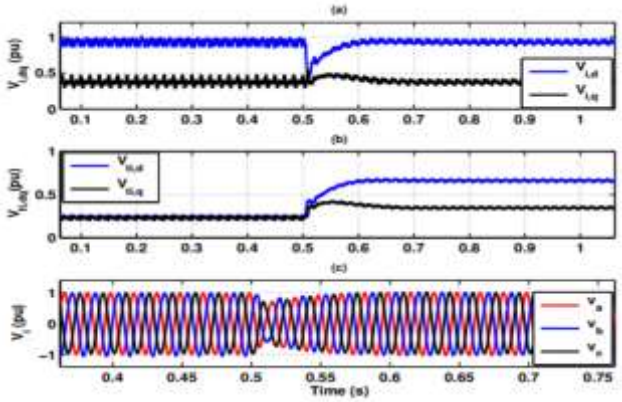

Fig. 5: Effective feedback of the simulation test network owing to an inductive load change: (a) dq-elements of the LV (b) dq voltage control inputs signal (c) instant LVs

Then, at t = 0.5 s, they rapidly drop to 5 mH. A variation in LC is considered in the last test. The system's second inductance load modification effective feedback signal is presented in Figure 5 (c), as shown between 0.5 s and 0.55 s. The three-phase LCs are abruptly altered from 850 F to 1700 F at roughly t = 1:1 s. In contrast, the LRs and load inductances are set based on the values listed in Table 1. Figure 5 shows the adequate reaction of the test network due to purely capacitive load.

3.1 Effective Implementation during Unusual Voltage Conditions

The controller efficiency has also been evaluated based on the system's performance during voltage imbalance at PCC 2. The imbalance voltages at PCC2 are shown in Figure 6 (a), obtained using a tracking set digital storage oscilloscope on Simulink. As displayed in Figures 6 (b) and (c), amelioration of the imbalance situation of the LV using UVTG and SRF controllers is insufficient. The stable condition of the LVs was attained after applying the recommended effective controller to the series VSI, as shown in Figure 6 (b) at t equal to

0.7 s for both d and q components. The findings indicate that the suggested series compensator controller has superior performance. It is critical to manage the LV under abnormal voltage situations at PCC2 to safeguard the loads that are voltage sensitive.

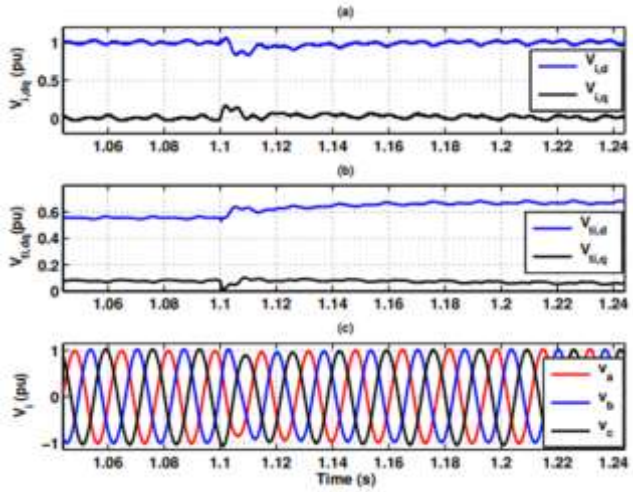

Fig. 6: Effective feedback of the results test network owing to a capacitive load variation: (a) dq-elements of the LV (b) dq voltage control inputs (c) instant LV

The Simulink implementation of the purported enhanced SRF theory centered on FNF for the studied network has been provided for different voltage disruptions such as under-voltage, over-voltage, and unbalanced voltage. As illustrated, the voltage signals at PCC2, which have an under-voltage from nominal 110 V to 60 V, have been measured. Figure 7 (b) shows the system's ability to adjust LVs in a sag condition. Figure 7 (c) also indicates interior added voltage signals, structured DCLV, and continuous PV current. In the final test, the effect of LC variation is investigated. In this regard, the LCs in the 3 phases were being rapidly shifted from the nominal value of 850 F to 1700 F at approximately t = 1.1s, while the LR and load inductances are set using the values provided in Table 1. Figure 7 depicts the test system's appropriate approach. The outcome of the result, in this case, is shown in Figure 7 (e) that voltage disruptions experienced in (a) to (b) are cleared out at the activation of FNF control architecture.

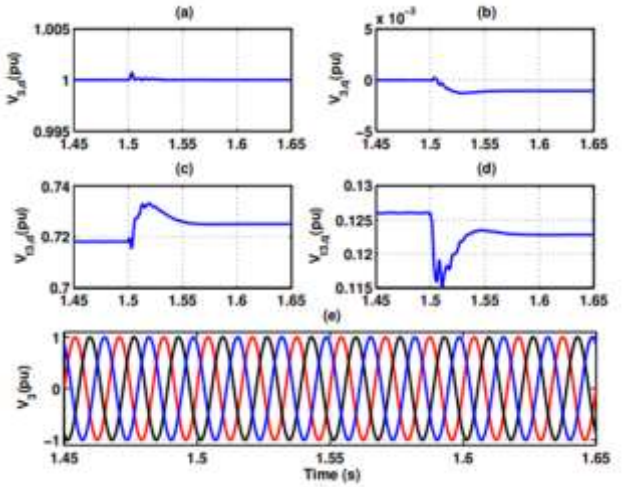

Fig. 7: The tracking reference pre-determine point: (a) d-element of LV at load centre (b) q-element of LV at load centre (c) d-element PV unit control signal (d) q-element PV unit control signal (e) instant PCC 2 LVs

The nominal network voltage is amplified to 149.9 V from 110 V, as indicated in Figure 8 (a), during a voltage rise situation, the quantified voltage at the connection point 2. As revealed in Figure 8 (b) and Figure 8 (c), the examined network proficiently controlled the DCLV and the load center. During voltage swells, grid current decreases to sustain real power balance, as indicated in Figure 8 (d). In the same figure, the point of connection 2 shows the network's decline in voltage harmonics. The suggested adaptive series VSI, as displayed in Figure 8 (e), regulates and maintains sinusoidal LVs. As presented in Figures 8 (b) and 8 (c), The system under consideration proficiently controlled the load and DCLV. During a voltage sag, grid current decreases to maintain active power balance, as depicted in Figure 8 (d). Figure 8 also shows the elimination of voltage harmonics at PCC 2. LVs are tightly controlled and maintained sinusoidal by the recommended influential series ameliorator, as depicted in Figure 8 (b).

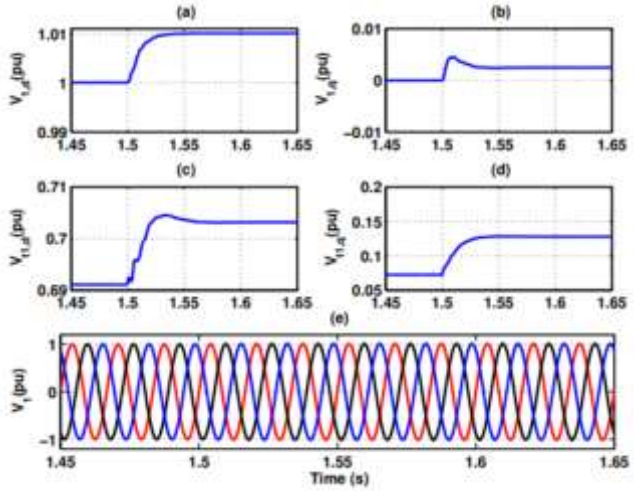

Fig. 8: The tracking reference pre-determine point: (a) d-element at PCC1 for LV (b) q-element at PCC1 for LV (c) d-element of PV unit control signal (d) q-element of PV unit control signal (e) instant LVs

3.2 Effective Execution under Load Unbalancing Condition

Appearance unbalance load occurs at PCC2 when one load is removed abruptly, as seen in Figure 9 (a). The load power requirement is reduced with the separation of a single-phase load. As a consequence, an upsurge in system current is seen in Figure 9 (a), indicating that the real power stability is being maintained. In the current realistic scenario, this graph illustrates the regulator's capacity to maintain the source current sinusoidal. Figure 9 (b) depicts the effectiveness under nonlinear load addition at a single phase. The significant raise in load power required by the end user causes a reduction in grid current measured at the connection point 2. Regardless of whether the load is isolated and added easily, the matching phase-A' current remains sinusoidal. The output power of the PV then fluctuates as a result of a shift in its local load. Because PV units contribute to lowering overall power requirements, the Synchronous Reference Frame (SRF) controller assigns the following new setpoints for each Photovoltaic module at t = 1.49s: $v_{1,dqref} = 1.01\angle 0.14^0$, $v_{1,dqref} = 1\angle 0^0$, and $v_{3,dqref} = 1\angle 0.06^0$. Figure 9 (e) displayed the response of each PV unit due to the setpoint changes.

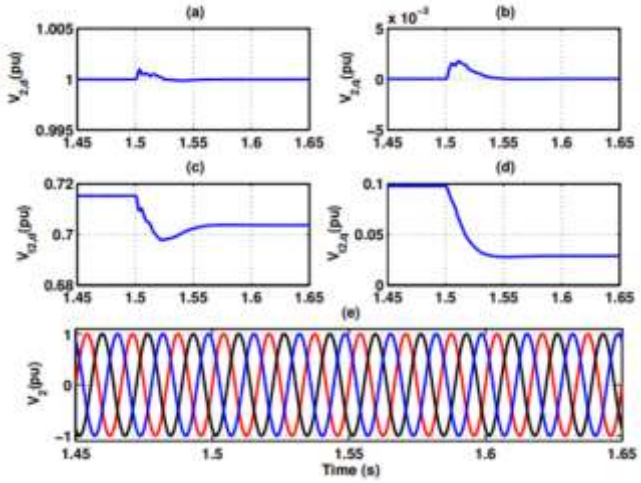

Fig. 9: Tracking reference set-point at: (a) d-element at PCC2 for LV (b) q-element at PCC 2 for LV (c) d-element of PV unit control signal (d) q-element of PV unit control signal (e) instant PCC2 LVs.

3.3 Execution during Stochastic in Solar Irradiations

The PV-IUPQC device's performance under practical settings of solar irradiation variability is examined in this section. The system's performance was evaluated under two different types of solar irradiation. The drop in solar irradiation from 1000 to 600 W/m^2 is seen in Figure 10 (a). In Figure 10 (a), the reduction in grid current at PCC1 with decreasing irradiation is visible. In Figure 10 (b), a boost in solar intensity from 600 to 1000 W/m^2 has also been observed. As shown in Figure 10 (b), a rise in grid currents is associated with an increase in irradiation.

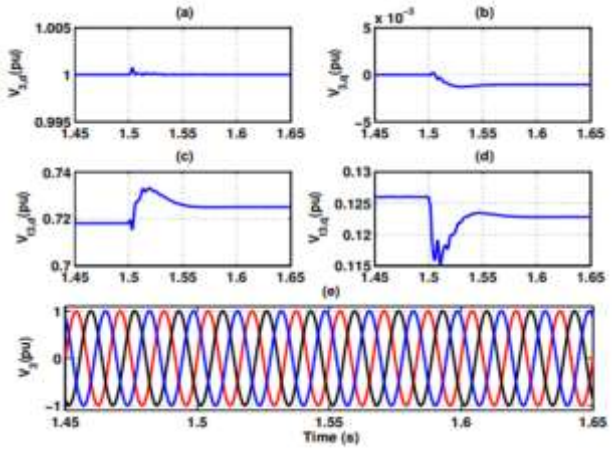

Fig. 10: Reference pre-determines tracking for stochastic in solar PV: (a) d-element at PCC1 for LV (b) q-element at PCC1 for LV (c) d-element of PV unit control signal (d) q-element of PV unit control signal (e) instant LVs

4 Prototype Development and Execution

As illustrated in Figure 4, the PV-O-UPQC system hardware prototype was created using a Solar PV Array simulator, multiple voltage source ameliorators, a VSL, and a programmable AC source. Hall effect transducers (sensors LV35-P, current sensors LA66-P) are used to detect analog signals, which are sent into a DSP processor for UPQC system control. The DSP processor has been used to implement the developed control algorithms. The PV-UPQC performance was assessed using a power analyzer and a digital storage oscilloscope. To study and authenticate the efficacy, and performance of the created system under a variety of active situations, extensive tests were done using chosen parameters as shown in Table 1.

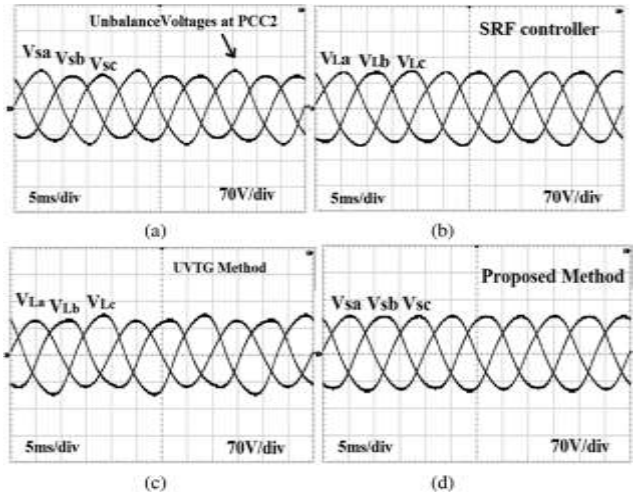

Fig. 11: Experimental outcome due to unbalance voltage condition: (a) dq-element of voltage at PCC 2, (b) regulated LV with SRF regulator, (c) LV regulated with UVTG controller, (d) regulated voltage with the intended regulator.

4.1 Experimental Implementation during Unusual Voltage Conditions

The controller efficiency has also been evaluated based on the system's performance under voltage unbalance at PCC2. The unbalanced voltages at PCC2 are shown in Figure 11 (a), which were obtained using a RIGOL-1153Z digital storage oscilloscope. As depicted in Figures 11 (b) and (c), amelioration of the unbalanced state of the LV applying SRF controller is insufficient. The LVs were compensated after installing the proposed efficient regulator to the control circuit, as depicted in Figure 11. (d). The collected findings indicate that the suggested series ameliorator controller has improved performance. To protect VSLs at PCC 2, during abnormal voltage conditions, it is critical to adjust the LV. For different voltage disruptions such as undervoltage, overvoltage, and unbalanced voltage, the active functioning of the recommended improved SRF theory based on FNF for the researched system is presented. The voltage signals at the connection point 2 exhibit a voltage sag ranging from nominal 110 to 60 V, as shown in Figure 12 (a). Figure 12 (a) depicts the system's capability to modify LVs in low-voltage situations. Figure 12 shows that the currents at the connection point 2 have enhanced to retain power balance throughout an undervoltage scenario. (d). Internal signals such as infused voltage monitored DCLV and current flowing in solar PV are also shown in Figure 12 (c).

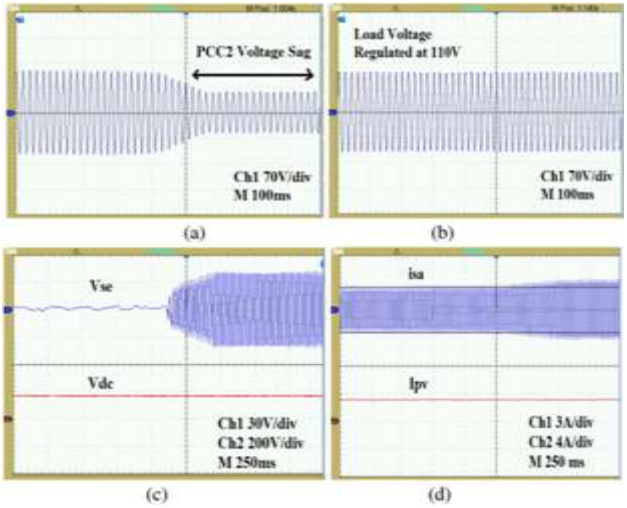

Fig. 12: Experimental under voltage situation: (a) voltage magnitude at PCC 2, (b) regulated LV, (c) VSC series injected voltage, DCLV, (d) PCC 2 current, PV current.

The measured voltage at PCC2 in an over-voltage situation, in which the nominal grid voltage is raised to 150 V from 110, is displayed in Figure 13 (a). As shown in Figure 13 (b) and Figure 13 (c), the investigated system effectively controlled the DCLV and LV. The grid current drops during a voltage swell to maintain the balance of active power, as shown in Figure 13 (d).
In Figure 14, the reduction of voltage harmonics at PCC2 is also seen. The suggested effective series ameliorator, as illustrated in Figure 14 (b) regulates and maintains sinusoidal LVs.

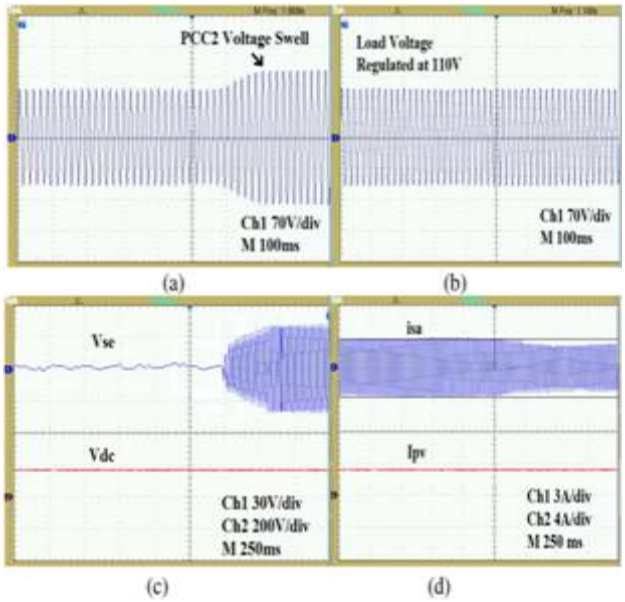

Fig. 13: Experimental over-voltage situation: (a) voltage magnitude at PCC 2, (b) LV regulated, (c) VSC series delivered voltage, DCLV, (d) PCC 2 current, PV array current.

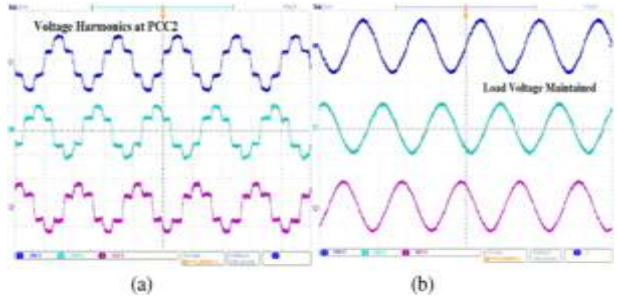

Fig. 14: Harmonics voltage condition: (a) the PCC 2 voltage with harmonics, (b) regulated LV.

4.2 Experimental Execution under Load Unbalancing Condition

Presence load unbalancing occurs at PCC 1 when a single-phase load is removed abruptly, as seen in Figure 15 (a). The disengagement of a single-phase load reduces the load's power requirement. To preserve the real power balance, an increase in grid current is seen, in Figure 15 (a). The controller's efficiency in maintaining the sinusoidal source currently under the current dynamic state is shown in this diagram.

Similarly, as illustrated in Figure 15 (b), single-phase performance under nonlinear load addition has been investigated. The increase in load power demand caused a load increase at the consumer end resulting in a drop in current at the grid recorded at PCC 1. The matching phase a' current remains sinusoidal even when the load is removed and added suddenly.

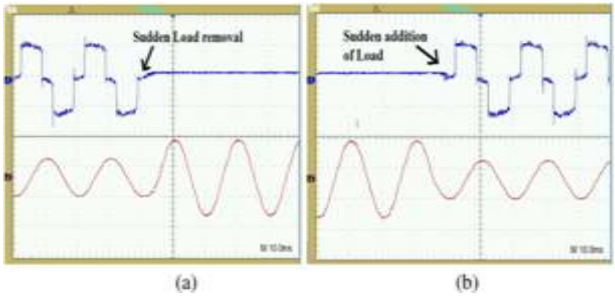

Fig. 15: Load unbalancing situation: (a) unexpected load disconnection, (b) instant load connection.

4.3 Experimental Execution Stochastic Variation in Solar Irradiations

This section looks at the PV-UPQC system's performance under solar irradiation fluctuations. The system's performance was measured under two different solar irradiation scenarios. Figure 16 (a) shows the decrease in solar irradiation from 1000 to 600 W/m^2. Figure 16 (a) shows that the drop in grid current at PCC1 with decreasing irradiation is visible. In Figure 16 (a), a surge in solar irradiation from 600 to 1000 W/m has also been observed. In this case, as shown in Figure 16 (b), the grid currents increase is associated with an increase in irradiation.

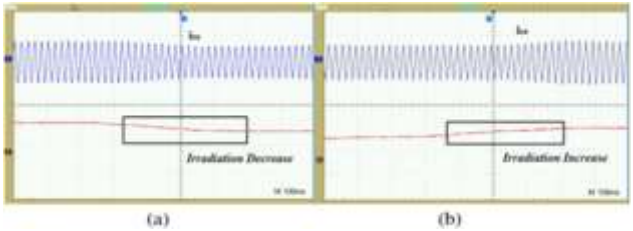

Fig. 16: Solar irradiations variation situation: (a) decline in current, and irradiation, (b) Rise in current, and irradiation.

5 Discussion

Overall, the effectiveness of the architectural control design was justified through the obtained simulation and experimental results. In all conditions the control is subjected to it proves very robust and flexible. Under the PV-UPQC system's performance under solar irradiation fluctuations, the decrease in solar irradiation from 1000 to 600 W/m2 shows that the drop in grid current at PCC1 with decreasing irradiation is visible. Also, a surge in solar irradiation from 600 to 1000 W/m has been observed, In this case, grid currents increase is associated with an increase in irradiation.

6 Conclusion

The evolution and execution of the PV-IUPQC were presented in this work. The main focal point was the improvement of the PQ in the presence of several voltage disturbance issues. The regulated architecture gives the consumer the option of selecting the power quality (PQ) level that corresponds to their requirements. The generated adequate RS in severe voltage disruptions, a synchronous reference frame (SRF) regulator based on a flexible notch filter (FNF) was used. This allows the consumer to operate at different PQ levels within the network. The suggested Logarithmic Absolute (LA) algorithm determines the effective decisive component of the basic LC. The use of ATF as a low pass filter (LPF) substitute for dc bus voltage decreases the chance of high and low-frequency ripple. The proposed algorithm has substantiated the authenticity of the simulation outcomes. Likewise, the effectiveness of the architectural control design was justified through the obtained simulation results. Finally, the results obtained from the experiment indicate that the new approach delivers a reasonable, effective performance in the toughness of PV-IUPQC at load parameters variations and voltage tracking from PV according to IEEE standard 45. An optimal implementation of the control architecture can be developed in subsequent research to accommodate the stochastic nature of the PV source to produce better results.

References:

[1] A. Javadi, M. Abarzadeh, L.-A. Grégoire, and K. Al-Haddad, "Real-Time HIL Implementation of a Single-Phase Distribution Level THSeAF Based on D-NPC Converter Using Proportional-Resonant Controller for Power Quality Platform," *IEEE Access*, vol. 7, pp. 110372–110386, 2019, doi: 10.1109/ACCESS.2019.2934033.

[2] T. Thenmozhi, M. V. S. Devi, and S. Kavitha, "Improvement of Power Quality Using PV with UPQC," in *2022 8th International Conference on Smart Structures and Systems (ICSSS)*, 2022, pp. 1–6, doi: 10.1109/ICSSS54381.2022.9782210.

[3] B. Singh and R. Kumar, "A comprehensive survey on enhancement of system performances by using different types of FACTS controllers in power systems with static and realistic load models," *Energy Reports*, vol. 6, pp. 55–79, 2020.

[4] O. Osaloni, A. S.-J. of E. R. in Africa, and undefined 2020, "Voltage Dip/Swell Mitigation and Imaginary Power Compensation in Low Voltage Distribution Utilizing IUPQC(I-UPQC)," *Trans Tech Publ*, Accessed: Feb. 20, 2023. [Online].

[5] M. K. Singh and V. Saxena, "Voltage Conditioning and Harmonic Mitigation Using UPQC: A Review," *Innov. Cyber Phys. Syst.*, pp. 523–534, 2021.

[6] S. Narula, B. Singh, G. Bhuvaneswari, and R. Pandey, "Improved Power Quality Bridgeless Converter-Based SMPS for Arc Welding," *IEEE Trans. Ind. Electron.*, vol. 64, no. 1, pp. 275–284, 2017, doi: 10.1109/TIE.2016.2598519.

[7] M. A. Mansor, K. Hasan, M. M. Othman, S. Z. B. M. Noor, and I. Musirin, "Construction and performance investigation of three-phase solar PV and battery energy storage system integrated UPQC," *IEEE Access*, vol. 8, pp. 103511–103538, 2020.

[8] R. Senapati, R. K. Sahoo, S. Pradhan, and R. N. Senapati, "Sinusoidal current control strategy for 3-phase shunt active filter in grid-tied PV system," in *2017 International conference on energy, communication, data analytics and soft computing (ICECDS)*, 2017, pp. 1272–1277.

[9] O. O. Osaloni and A. K. Saha, "Voltage Dip/Swell Mitigation and Imaginary Power Compensation in Low Voltage Distribution Utilizing IUPQC(I-UPQC)," in *International Journal of Engineering Research in Africa*, 2020, vol. 49, pp. 84–103.

[10] O. O. Osaloni and L. Augustine, "Impact of Irregular Renewable Power Sources on the Grid Power Factor at Changeable Load Conditions," in *2022 30th Southern African Universities Power Engineering Conference (SAUPEC)*, 2022, pp. 1–6, doi: 10.1109/SAUPEC55179.2022.9730736.

[11] O. O. Osaloni and A. K. Saha, "Impact of IUPQCAllocation in Radial Distribution Network," *Int. J. Eng. Res. Africa*, vol. 59, pp. 135–150, 2022.

[12] D. A. Fernandes, F. F. Costa, J. R. S. Martins, A. S. Lock, E. R. C. Da Silva, and M. A. Vitorino, "Sensitive LV Compensation Performed by a Suitable Control Method," *IEEE Trans. Ind. Appl.*, vol. 53, no. 5, pp. 4877–4885, Sep. 2017, doi: 10.1109/TIA.2017.2715173.

[13] S. K. Dash and P. K. Ray, "A New PV-Open-UPQC Configuration for VSLs Utilizing Novel Adaptive Controllers," *IEEE Trans. Ind. Informatics*, vol. 17, no. 1, pp. 421–429, 2021,

[14] K. Onitsuka *et al.*, "Cardiac phase-targeted dynamic load on left ventricle differentially regulates phase-sensitive gene expressions and pathway activation," *J. Mol. Cell. Cardiol.*, vol. 64, pp. 30–38, Nov. 2013,

[15] O. O. Osaloni and A. K. Saha, "Distributed Generation Interconnection with IUPQCfor Power Quality Mitigation," in *2020 International SAUPEC/RobMech/PRASA Conference*, 2020, pp. 1–6.

[16] B. A. Angélico, L. B. G. Campanhol, and S. A. O. da Silva, "Proportional--integral/proportional--

integral-derivative tuning procedure of a single-phase shunt active power filter using Bode diagram," *IET Power Electron.*, vol. 7, no. 10, pp. 2647–2659, 2014.

[17] B. Z. Adewole, B. O. Malomo, O. P. Olatunji, and A. O. Ikobayo, "Simulation and experimental verification of electrical power output of a microcontroller based solar tracking photovoltaic module," *Int. J. Sustain. Energy Environ. Res.*, vol. 9, no. 1, pp. 34–45, 2020.

[18] R. T. Hock, Y. R. de Novaes, A. L. Batschauer, R. T. Hock, Y. R. de Novaes, and A. L. Batschauer, "A Voltage Regulator for Power Quality Improvement in Low-Voltage Distribution Grids," *ITPE*, vol. 33, no. 3, pp. 2050–2060, Mar. 2018,

[19] H. Nazaripouya and S. Mehraeen, "Modeling and Nonlinear Optimal Control of Weak/Islanded Grids Using FACTS Device in a Game Theoretic Approach," *IEEE Trans. Control Syst. Technol.*, vol. 24, no. 1, pp. 158–171, Jan. 2016,

[20] N. Gowtham and S. Shankar, "UPQC: A Custom Power Device for Power Quality Improvement," *Mater. Today Proc.*, vol. 5, no. 1, pp. 965–972, Jan. 2018,

[21] A. Agrawal, P. Agarwal, and P. Jena, "Compensation of voltage flicker using Unified Power Quality Conditioner (UPQC)," *2014 IEEE Int. Conf. Power Electron. Drives Energy Syst. PEDES 2014*, Feb. 2014

[22] A. Stephen Akinyemi, K. Musasa and I. E. Davidson, "Analysis of voltage rise phenomena in electrical power network with high concentration of renewable distributed generations," Scientifc Reports, vol. 12, p. 7815, 2022

[23] S. Dash, P. R.-(Springer S. & B. M. BV), and undefined 2018, "Design and Modeling of Single-Phase PV-UPQC Scheme for Power Quality Improvement Utilizing a Novel Notch Filter-Based Control Algorithm: An Experimental," *search.ebscohost.com*, Accessed: Jan. 31, 2023. [Online].

[24] S. Devassy, B. S.-I. T. on Industry, and undefined 2017, "Design and performance analysis of three-phase solar PV integrated UPQC," *ieeexplore.ieee.org*, Accessed: Jan. 31, 2023. [Online].

[25] M. H. Ahmadi *et al.*, "Evaluation of electrical efficiency of photovoltaic thermal solar collector," *Eng. Appl. Comput. Fluid Mech.*, vol. 14, no. 1, pp. 545–565, 2020.

[26] O. Osaloni and K. Awodele, "Analytical Approach for Optimal Distributed Generation Allocation in Primary Distribution Networks," in *Proc. 2016 South African Universities Power Engineering Conference*, pp. 115–120.

[27] O. O. Osaloni and A. K. Saha, "Impact of Improved Unified Power Quality Conditioner Allocation in Radial Distribution Network," *Int. J. Eng. Res. Africa*, vol. 59, pp. 135–150, 2022.

[28] D.B. Aeggegn, A.O. Salau, Y.W. Gebru, T.F. Agajie, "Mitigation of Reactive Power and Harmonics in a Case of Industrial Customer," *International Journal of Engineering Research in Africa*, Vol. 60, pp. 107-124, 2022.

[29] H. Firoozi and M. Imanieh, "Improvement performance CIGS thin film solar cells by changing the thickness Cd_S layer," *J. Res. Sci. Eng. Technol.*, vol. 6, no. 03, pp. 11–14, 2018.

[30] Y.P. Xu, P. Ouyang, S.M. Xing, L.Y. Qi, H. Jafari, and others, "Optimal structure design of a PV/FC HRES using amended Water Strider Algorithm," *Energy Reports*, vol. 7, pp. 2057–2067, 2021.

[31] C. U. Eya, A. O. Salau, S. L. Braide, S. B. Goyal, V. A. Owoeye, And O. O. Osaloni, "Assessment of Total Harmonic Distortion in Buck-Boost DC-AC Converters using Triangular Wave and Saw-Tooth based Unipolar Modulation Schemes" WSEAS Transactions on Power Systems 17, pp. 324-338, 2022.

Contribution of Individual Authors to the Creation of a Scientific Article (Ghostwriting Policy)

The authors equally contributed in the present research, at all stages from the formulation of the problem to the final findings and solution.

Sources of Funding for Research Presented in a Scientific Article or Scientific Article Itself

No funding was received for conducting this study.

Conflict of Interest

The authors have no conflicts of interest to declare that are relevant to the content of this article.

Creative Commons Attribution License 4.0 (Attribution 4.0 International, CC BY 4.0)

This article is published under the terms of the Creative Commons Attribution License 4.0
https://creativecommons.org/licenses/by/4.0/deed.en_US